Angular color shift of micro-LED displays

FANGWANG GOU,[1] EN-LIN HSIANG,[1] GUANJUN TAN,[1] PEI-TING CHOU,[2] YUN-LI LI,[2] YI-FEN LAN,[1] AND SHIN-TSON WU[1,*]

[1]*CREOL, The College of Optics and Photonics, University of Central Florida, Orlando, FL 32816, USA*
[2]*PlayNitride, Inc., Hsinchu 30288, Taiwan*
*swu@creol.ucf.edu

Abstract: Sidewall emission of a micro-scale light emitting diode (micro-LED) improves the light extraction efficiency, but it causes mismatched angular distributions between AlGaInP-based red micro-LED and InGaN-based blue/green counterparts due to material difference. As a result, color shift of RGB micro-LED displays may become visually noticeable. To address this issue, we first analyze the angular distributions of RGB micro-LEDs and obtain good agreement between simulation and experiment. Next, we propose a device structure with top black matrix and taper angle in micro-LEDs, which greatly suppresses the color shift while keeping a reasonably high light extraction efficiency.

1. Introduction

Micro-scale light emitting diode (micro-LED) is a potentially disruptive display technology because of its outstanding features such as high dynamic range, good sunlight readability, long lifetime, low power consumption, and wide color gamut [1–3]. To achieve full-color displays, two methods are commonly used: 1) color conversion, e.g. using blue (B) or ultraviolet (UV) micro-LEDs to pump green (G) and red (R) quantum dots or phosphors [4–6], and 2) to assemble individual RGB micro-LED pixels from semiconductor wafers to the same driving backplane through pick-and-place approach, which is referred to as mass transfer process. Although it is still challenging to achieve high manufacturing yield, a large-size display consisting of full-color micro-LED modules is emerging, such as microdisplays, tablets, monitors, TVs, and video walls [7,8].

For a micro-LED, as the chip size down to micron scale, although the internal quantum efficiency may droop due to increased non-radiative recombination from sidewall defects, its light extraction efficiency is improved because the light emission from sidewall gradually increases [9–12]. However, the far-field radiation pattern would deviate from ideal *Lambertian* distribution, depending on the sidewall emission intensity, which is determined by the refractive index of the employed semiconductor material and device structure. For commercial LEDs, the most commonly used epitaxy wafer for red LED is based on GaInP/AlGaInP multi-quantum wells (MQWs), while blue and green LEDs are based on InGaN/GaN MQWs [13,14]. Therefore, angular distribution mismatch among RGB micro-LEDs would occur because the red chip uses different epitaxy materials and has different structures from the green and blue ones. As a result, the angular color shift of mixed colors, such as skin tone, by mixing RGB colors with different ratios may become distinguishable by the human eye [15].

In this paper, we first analyze the color shift of RGB micro-LED displays originated from mismatched angular distribution. Next, we validate our simulation model with experiment, and obtain a good agreement. In order to reduce color shift, we propose a device structure with top black matrix. By introducing a taper angle in micro-LEDs, the light extraction efficiency can be improved simultaneously.

2. Simulation model and experiment

In our analysis, we examine the emission patterns of RGB micro-LEDs at different viewing angles with ray-tracing software LightTools. Table 1 lists the commonly used major structure layers and their thicknesses of flip-chip RGB chips. For AlGaInP-based red micro-LED, it has metal contact layer, n-cladding AlGaInP, n-type AlInP diffusion barrier, GaInP/AlGaInP MQWs, p-type AlInP diffusion barrier, p-cladding AlGaInP, and p-GaP window layer [16]. For InGaN-based green and blue micro-LEDs, their structures consist of metal contact layer, p-type GaN, AlGaN electron block layer, InGaN/GaN MQWs and n-type GaN. Although only the refractive indices at central wavelength are included here, during simulations the wavelength dispersion of refractive index for each material [17,18] is also considered. The die sizes are all 35 × 60 µm in order to be comparable to some commercial products. For simplicity, the metal pad is set to be the same size as chip size. Please note that the layout and materials for blue and green micro-LED are similar, but they are quite different from those of red chip. Light radiation from the multi-quantum wells (MQWs) with uniform angular distribution travels through each layer and across interfaces according to Snell's law.

Table 1. Optical parameters of commonly used AlGaInP-based red micro-LED and InGaN-based blue and green micro-LEDs adopted in simulations.

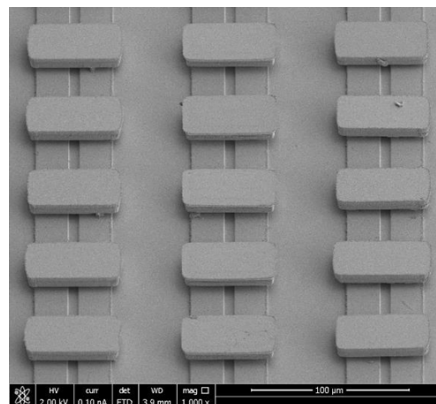| Red Layers	Thickness (µm)	n	k	Green/Blue Layers	Thickness (µm)	n Green	n Blue	k Green	k Blue
ITO	0.1	2.07	0	n-GaN	2.5	2.38	2.43	4e-5	4e-5
p-GaP	1.0	3.33	0	MQW	0.1	2.41	2.49	2e-2	2e-2
p-AlGaInP	0.1	3.30	0	p-AlGaN	0.05	2.31	2.35	6e-4	7e-4
p-AlInP	0.6	3.21	0	p-GaN	0.3	2.38	2.43	4e-5	4e-5
MQW	0.4	3.60	0.16	n/p-Metal	0.5	0.44	1.43	2.29	1.85
n-AlInP	0.3	3.21	0	-	-	-	-	-	-
n-AlGaInP	1.2	3.30	0	-	-	-	-	-	-
n/p-Metal	0.5	0.15	3.52	-	-	-	-	-	-

2.2 Emission spectra and angular distributions

Fig. 1. SEM image of RGB micro-LEDs arrays after transfer.

To validate our model, we fabricated RGB micro-LEDs with the same chip size 35 × 60 µm (Fig. 1), and measured the emission spectra of RGB chips from normal direction to 60°

viewing angle. Results are plotted in Figs. 2(a)-2(c). For each device, the central wavelength does not shift as viewing angle increases, indicating the cavity effect inside micro-LEDs is negligible. The central wavelength and full width at half maximum (FWHM) for RGB chips are [626 nm, 14 nm] for red, [529 nm, 34 nm] for green, and [465 nm, 16 nm] for blue. It should be mentioned here that organic LED intentionally utilizes the cavity effect to narrow the emission spectra, but the tradeoff is noticeable color shift [15].
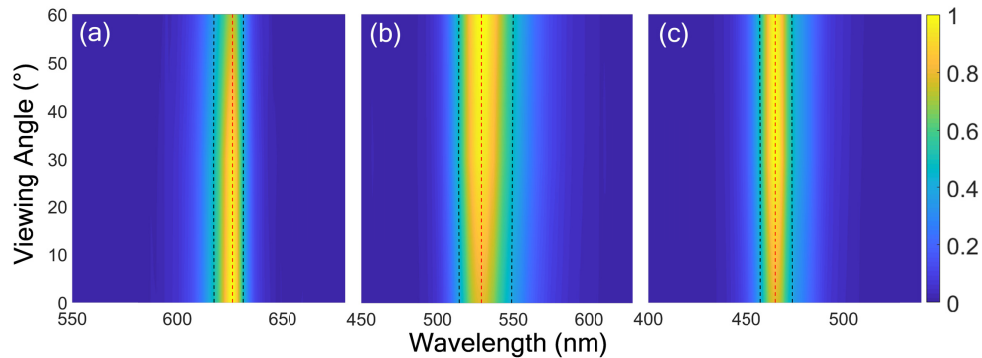

Fig. 2. Measured emission spectra of (a) red, (b) green, and (c) blue micro-LEDs at different viewing angles. Red and black dashed lines indicate the central wavelength and FWHM at each viewing angle.

Figure 3 shows the far-field radiation patterns of our RGB micro-LEDs. Dots represent the measured data and solid lines stand for simulation results. From Fig. 3, good agreement between experiment and simulation is obtained. As viewing angle increases, the light emission from red chip declines following *Lambert*'s cosine law. In contrast, for green and blue micro-LEDs, the light intensity gets stronger from normal angle to ~40° and then decreases. The mismatched angular distributions originate from different materials of RGB chips and will cause angular color shift of mixed colors, which will be discussed later.
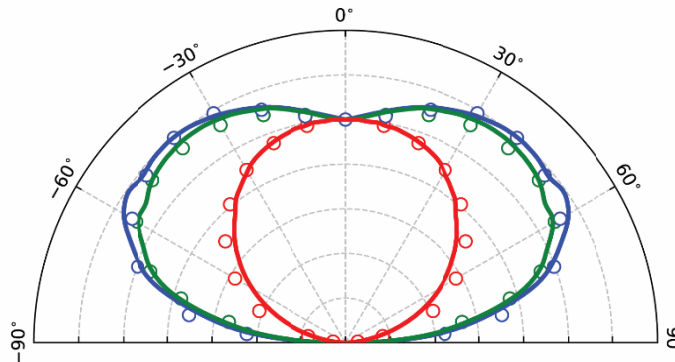

Fig. 3. Measured and simulated far-field radiation patterns of RGB micro-LEDs. Dots are experimental data and lines are simulation results.

3. Results and discussion

3.1 Sidewall emissions

For a traditional LED with chip size at millimeter scale, the light emission from top surface dominates, which is limited by total internal reflection. The critical angle (θ_c) between the semiconductor and air interface determines the amount of light escaping from LED and it can be calculated according to Snell's Law:

$$\theta_c = \sin^{-1}(\frac{n_{air}}{n}). \tag{1}$$

In Eq. (1), n_{air} and n represents the refractive index of the air and top semiconductor layer, respectively. If we neglect the Fresnel loss at semiconductor/air interface, the light extraction efficiency η of the LED can be estimated using following equation [19]:

$$\eta = \frac{\Omega}{4\pi}, \tag{2}$$

where Ω is the solid angle of escape cone, which is expressed as:

$$\Omega = \int_0^{2\pi} d\phi \int_0^{\theta_c} \sin\theta d\theta. \tag{3}$$

However, as the chip size shrinks, the sidewall emission from micro-LED should also be taken into consideration. In other words, after photons are generated from the MQWs, they can be extracted from all of six surfaces of the chip. Figures 4(a)-4(c) depict the simulated total, top and sidewall emissions from RGB micro-LEDs. As can be seen, the top emissions of RGB chips are all *Lambertian* distributions, but the sidewall emission from green and blue chips are much stronger than that from red one. This difference originates from the stronger absorption of red MQW than that of green and blue MQWs.
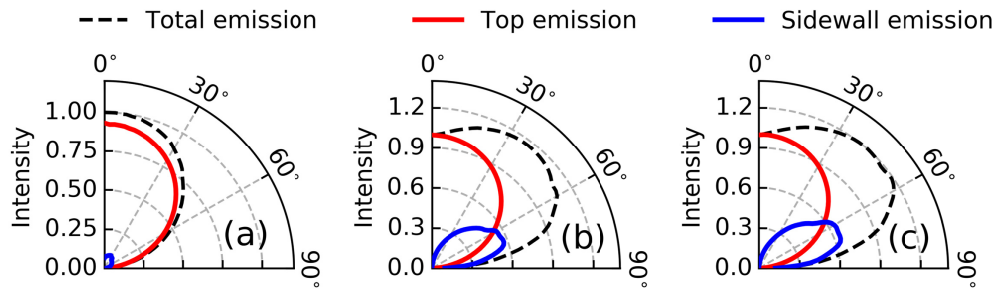

Fig. 4. Simulated total, top, and sidewall emissions of (a) red, (b) green, and (c) blue micro-LEDs at different viewing angles.

To analyze the light path inside the micro-LED, we take a point-like source located at MQW layer with coordinate (x, y) as an example (Fig. 5(a)). The chip size is $l \times w$ and the distance of MQW from top surface is h_1. On the top surface, the light can be extracted for the rays with the angle of incidence θ_i smaller than θ_c, as depicted by the black line in Fig. 5(b). We can obtain a completed escape cone due to the short distance h_1 between MQW and the semiconductor/air interface. The top emission ratio to the total emission intensity can be calculated using Eq. (2). In the opposite direction, the light goes downward and gets reflected by the bottom electrode pad back to top surface [i.e. yellow line in Fig. 5(b)], which should be also included as top emission. But for the downward light, both reflectance R_s of bottom metal pad and absorption of MQW need to be taken into consideration during calculation.
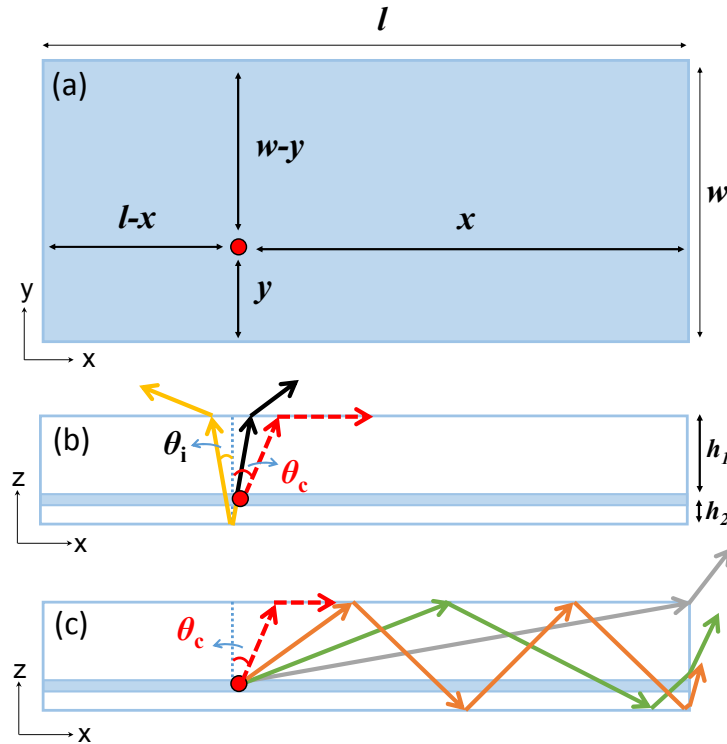
Fig. 5. (a) Top view of micro-LED chip with a point-like source located at (x, y). (b, c) Side views of light emission from the point source with emission angle θ_i: (a) $\theta_i < \theta_c$: top emission; (c) $\theta_i > 90° - \theta_c$: sidewall emissions.

For the emission towards sidewall, the escape cone may not be completed, depending on the position of point-like sources located at the MQW layer. For example, the point source at a short distance from sidewall can get a completed escape cone. However, as the distance increases, the escape cone will become uncompleted because of the small thickness of micro-LED chip (< 4 μm). Figure 5(c) shows the side-view of light emissions from the point source with angle θ_i satisfying $90° - \theta_c < \theta_i < 90°$. Light within this angle range will escape from the sidewall but experience different absorption or reflection losses. For example, when the light emission from the point source reaches the top edge of the sidewall without experiencing reflection [gray line in Fig. 5(c)], we can obtain a light escape cone $\theta_1 = \tan^{-1}(h_1/x)$ without absorption and reflection loss. The emission ratio can be calculated using Eqs. (2) and (3). If the emission angle θ_i satisfies $90° - \theta_c < \theta_i < 90° - \theta_1$, although the light can still escape from sidewall, it will experience multiple reflections between top and bottom surfaces as well as absorption of MQW, which are illustrated by green and orange lines in Fig. 5(c). For the light reflected by the bottom surface n times, the sidewall emission ratio can be estimated by modifying Eqs. (2) and (3) as:

$$\eta_n = \frac{1}{2} e^{-2n\alpha d} R_s^{\ n} \int_{\theta_{n-1}}^{\theta_n} \sin\theta d\theta. \tag{4}$$

In Eq. (4), α and d represent the absorption coefficient and thickness of MQW layer, and R_s is the reflectance of bottom metal pad. For simplicity, we have neglected the Fresnel loss at semiconductor/air interface and the refraction between different layers inside micro-LED. Thus, the total sidewall emission ratio from four side surfaces can be calculated by adding all the ratios together. The calculated results by MATLAB and the simulated data using ray-tracing in LightTools for micro-LEDs with different chip size are listed in Table 2. The

agreement between these two methods is very good. As the chip size shrinks from 50×100 μm^2 to 15×30 μm^2, the sidewall emissions from RGB micro-LEDs increase because of lower absorption and reflection losses inside the chip. For red micro-LEDs, the sidewall emission ratio is much smaller than that from green and blue ones due to stronger absorption of red MQW, resulting in a mismatched angular distribution among RGB micro-LEDs.

Table 2. Simulated and calculated sidewall emission ratio for a RGB micro-LED display with different chip size.

Chip size (μm^2)	Red		Green		Blue	
	Sim.	Cal.	Sim.	Cal.	Sim.	Cal.
15×30	10.8%	11.0%	58.9%	58.5%	62.2%	65.7%
35×60	5.3%	5.6%	52.4%	54.2%	55.1%	56.7%
50×100	3.8%	4.0%	47.2%	49.6%	50.1%	52.9%

3.2 Color shift and light efficiency

To analyze the color shift induced by subpixels' angular distribution mismatch, a more representative way is to calculate the color shifts of the mixed colors by RGB color mixing. We have defined 10 reference colors in total in order to evaluate color shift throughout the entire color gamut. These reference colors include three primary colors, white point D65, and six mixed colors (three 100% saturated colors and three 50% saturated colors), which are plotted in CIE 1976 color space [20,21], as shown in Fig. 6.
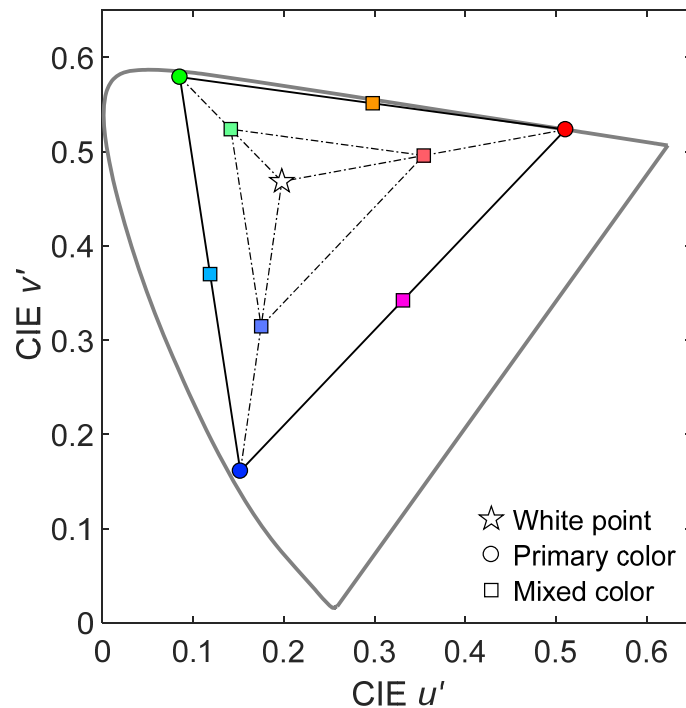

Fig. 6. 10 reference colors in CIE1976 color space, with D65 white point and RGB micro-LEDs primary colors.
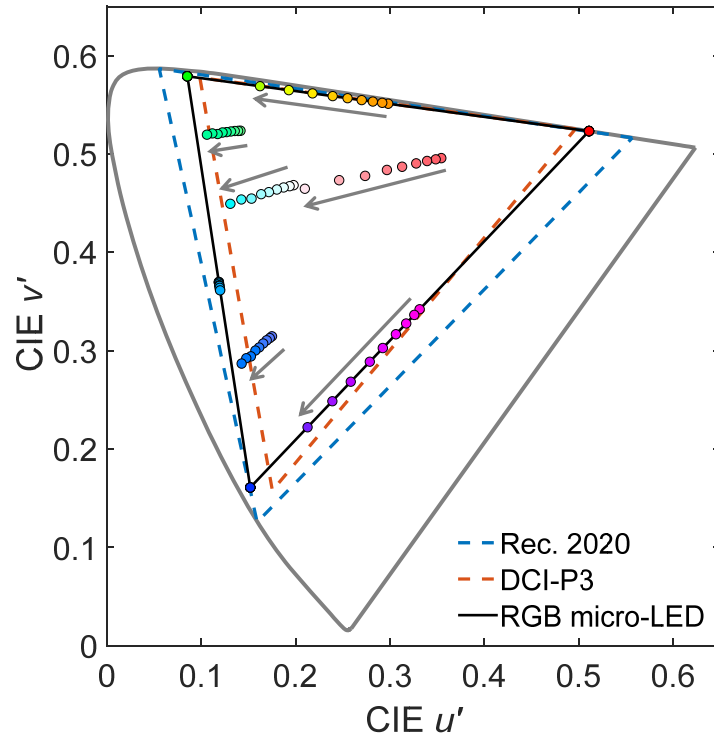
Fig. 7. Simulated color triangle of the RGB micro-LED display system and the CIE coordinates of 10 reference colors from 0° to 80° viewing angle. The arrows indicate the color shift as viewing angle changes.

Figure 7 depicts the color triangle of the RGB micro-LED display and CIE coordinates of 10 reference colors at viewing angles from 0° to 80° with 10° intervals. For primary colors, no color shift is observed at fixed driving current due to weak cavity effect inside micro-LEDs. While for mixed colors and white point, color shift becomes worse as viewing angle increases as expected. The average color shift $\Delta u'v'$ of all colors at 80° is 0.061 and the maximum value is 0.169 for magenta channel, which exceeds the just-noticeable level ($\Delta u'v'$ < 0.02). This issue will get worse as the micro-LED size decreases because of increased sidewall emissions from green and blue chips, as listed in Table 2. Therefore, it is necessary to improve the color performance of RGB micro-LED display system, especially for high resolution applications.

In terms of color gamut, our display device can cover 97% of DCI-P3 standard and 78% of Rec. 2020 standard, as indicated by the color triangle in Fig. 7. The relatively narrow color gamut coverage results from the spectral crosstalk between green and red chips, as Fig. 8 shows. Compared to our device, the Osram's green LED has a slightly shorter central wavelength and narrower FWHM. As a result, it has less crosstalk with the red LED and its RGB LED system can achieve wider color gamut. The calculated color gamut coverage is 99% of DCI-P3 standard and 90% of Rec.2020 standard. To achieve a desired color gamut, we can tune the electroluminescent (EL) spectrum of green micro-LED by controlling the well/barrier width and indium composition of MQWs [22].
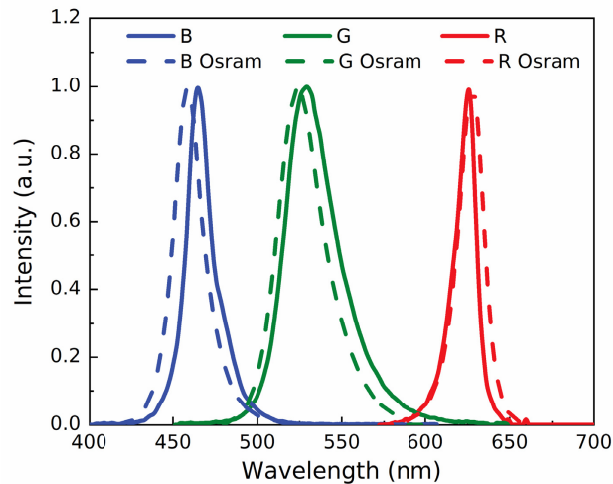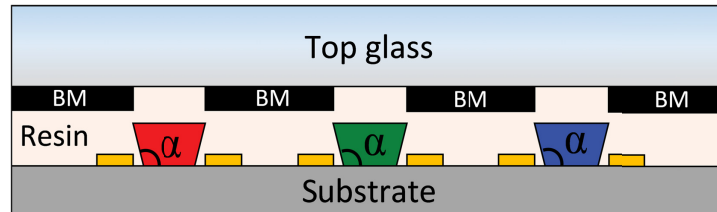
Fig. 8. RGB spectra of our and Osram's micro-LEDs.

Fig. 9. RGB micro-LED display with top black matrix.

To reduce color shift, a straightforward method is to obtain matched RGB radiation patterns, i.e. *Lambertian* distribution, which means the sidewall emissions from green and blue micro-LEDs should be eliminated. Figure 9 illustrates our proposed display configuration consisting of micro-LED array and top black matrix outside the emission region. The gap between micro-LEDs are filled with resin or other dioxide materials with refractive index of ~1.5. As a result, the sidewall emissions from green and blue chips can be completely absorbed by the black matrix, allowing only emissions from top surface of RGB micro-LEDs with matched *Lambertian* distributions. Thus, a negligible color shift can be obtained, but the trade-off is ~2x lower optical efficiency, because the sidewall emission ratios of green and blue chips contribute to ~50% of the total emission intensity, as listed in Table 2.

Since power consumption is another key performance metric for displays, we introduce a taper angle α in the micro-LED structure (Fig. 9) to improve the light intensity from top surface [23–25]. The simulated light intensity ratio is normalized to the device with right angle and without black matrix as Fig. 10 shows. As the taper angle α changes from 90° to 140°, the light intensity from green and blue chips first increases and then saturates, while that from red LED almost keeps steady. The color shift becomes severe even if the presence of black matrix when α is larger than 130°. This is because a larger taper angle causes a narrower angular distribution of top emissions for green and blue LEDs but it has little impact on the red counterpart. Thus, the mismatched angular distribution causes a severe color shift. By considering device fabrication, light efficiency as well as color shift, taper angle $\alpha = 120°$ is an optimal choice for green and blue chips. With this configuration, the light efficiency of green and blue micro-LEDs can be boosted to 83% and 86%, respectively, compared to the device with 90° taper angle but without black matrices, while keeping unnoticeable color shift.
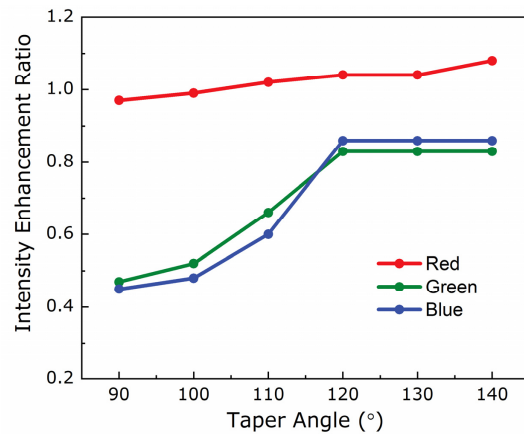
Fig. 10. Light intensity enhancement ratio normalized to bare RGB micro-LEDs (90° taper angle and without black matrix) as taper angle α changes.

The simulated color shifts for RGB micro-LED display with top black matrix and 120° taper angle is plotted in Fig. 11. The average $\Delta u'v'$ of all 10 reference colors at 80° is 0.005 and the maximum value is 0.014 for magenta channel, which is below 0.02 and is acceptable for commercial applications. Besides these 10 reference colors, we also evaluate the color shift using the first 18 colors in Macbeth ColorChecker [26], which is commonly used in color tests and reproductions to mimic the colors of natural objects such as human skin, foliage and flowers. Figure 12 depicts the simulated results. The color shifts of all 18 reference colors within 80° viewing cone are below 0.01 and the maximum average $\Delta u'v'$ is 0.007, which remains visually unnoticeable by human eye.
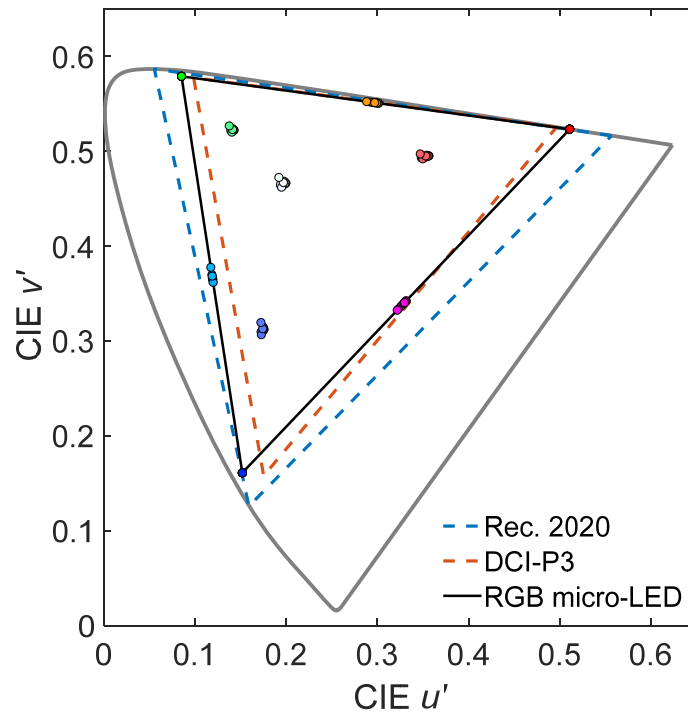

Fig. 11. Simulated color shifts of 10 reference colors from 0° to 80° viewing angle for RGB micro-LED display with top black matrix and 120° taper angle.
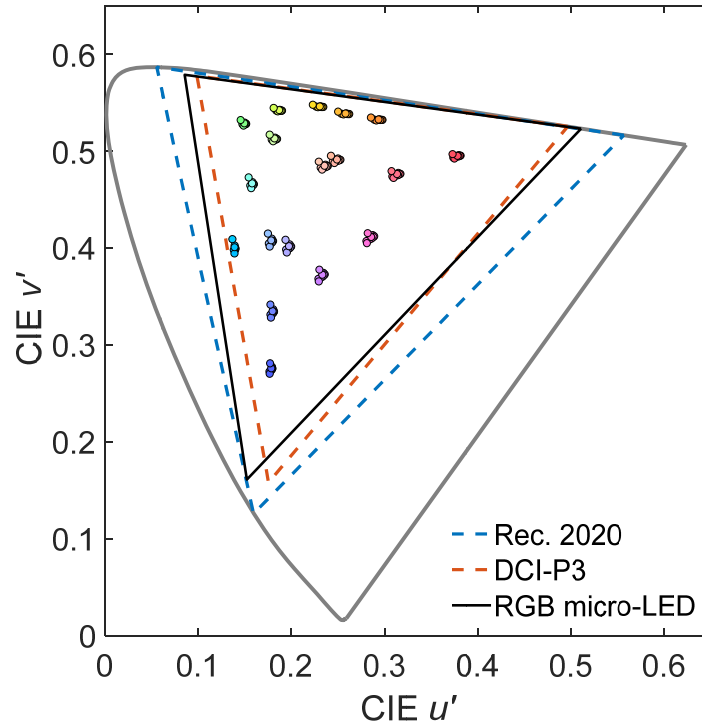
Fig. 12. Simulated color shifts of the first 18 colors in Macbeth ColorChecker from 0° to 80° viewing angle for RGB micro-LED display with top black matrix and 120° taper angle.
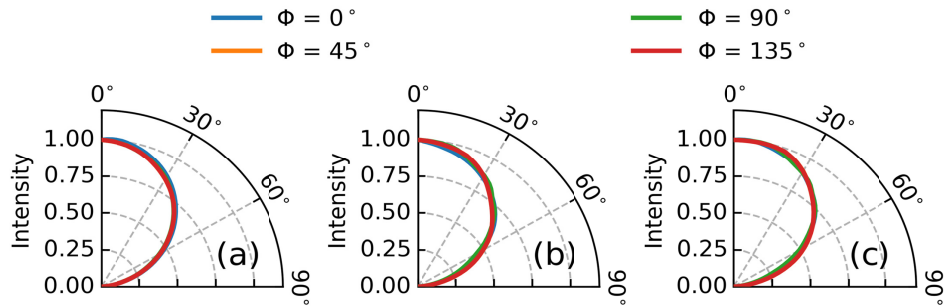
3.3 Discussion

Fig. 13. Simulated radiation patterns of (a) red, (b) green, and (c) blue micro-LEDs with top black matrix and 120° taper angle at different viewing angle θ and azimuthal angle φ.

In the above section, we have discussed the color shift of RGB micro-LED displays when the viewing angle θ (polar angle) changes along a fixed azimuthal angle (φ). It is noteworthy that the sidewall emission from a bare LED without black matrix will not stay the same when the azimuthal angle changes because it has a rectangular shape. As a result, the angular distributions would be different, leading to different levels of color shifts of RGB micro-LED display at different azimuthal angle. With the presence of black matrix, the color shift can be greatly suppressed at all polar angles and azimuthal angles because all the sidewall emissions are effectively absorbed and matched angular distributions for both RGB colors can be obtained, as shown in Fig. 13. In addition, the black matrices help to absorb the ambient light reflected from the micro-LED chips and metal wires, which in turn improves the ambient contrast ratio [27,28]. Other approaches to reduce angular color shift include making

asymmetric subpixel arrangement [29] or employing a patterned scattering film on top of the display panel to achieve matched angular distributions [30]. Each approach has its own merits and demerits.

In addition to angular color shift caused by angular distribution mismatch, micro-LED display may also suffer from color shift originating from spectral shift at different driving current densities. Due to the competition between band-filling effects and self-heating-induced bandgap shrinkage, blueshift at the low current density level and redshift at the high current density level have been reported [31,32]. This color shift issue might be addressed by image rendering, optimization of epitaxial wafer [33] or driving method, etc.

4. Conclusion

We have analyzed the color shift of RGB micro-LED displays due to angular distribution mismatch. The simulation model is validated by experiment and a good agreement is obtained. In order to mitigate the color shift while keeping a high light extraction efficiency, we proposed a device structure with top black matrix and taper angle in micro-LEDs. After optimization, the color shift $\Delta u'v'$ of the RGB micro-LED display with 120° taper angle is suppressed to below 0.01 within 80° viewing cone for the first 18 reference colors in Macbeth ColorCheker, and the efficiency keeps ~85% of the device without black matrix.

Funding

References

1. S. X. Jin, J. Li, J. Z. Li, J. Y. Lin, and H. X. Jiang, "GaN microdisk light emitting diodes," Appl. Phys. Lett. **76**(5), 631–633 (2000).
2. H. X. Jiang and J. Y. Lin, "Nitride micro-LEDs and beyond-a decade progress review," Opt. Express **21**(S3 Suppl 3), A475–A484 (2013).
3. Z. Liu, W. C. Chong, K. M. Wong, and K. M. Lau, "GaN-based LED micro-displays for wearable applications," Microelectron. Eng. **148**, 98–103 (2015).
4. H. V. Han, H. Y. Lin, C. C. Lin, W. C. Chong, J. R. Li, K. J. Chen, P. Yu, T. M. Chen, H. M. Chen, K. M. Lau, and H. C. Kuo, "Resonant-enhanced full-color emission of quantum-dot-based micro LED display technology," Opt. Express **23**(25), 32504–32515 (2015).
5. G. Chen, B. Wei, C. Lee, and H. Lee, "Monolithic red/green/blue micro-LEDs with HBR and DBR structures," IEEE Photonics Technol. Lett. **30**(3), 262–265 (2018).
6. F. Gou, E. L. Hsiang, G. Tan, Y. F. Lan, C. Y. Tsai, and S. T. Wu, "Tripling the optical efficiency of color-converted micro-LED displays with funnel-tube array," Crystals (Basel) **9**(1), 39 (2019).
7. E. H. Virey and N. Baron, "Status and prospects of microLED displays," SID Int. Symp. Digest Tech. Papers **49**(1), 593–596 (2018).
8. K. Ding, V. Avrutin, N. Izyumskaya, Ü. Özgür, and H. Morkoç, "Micro-LEDs, a manufacturability perspective," Appl. Sci. (Basel) **9**(6), 1206 (2019).
9. H. W. Choi, C. W. Jeon, M. D. Dawson, P. R. Edwards, R. W. Martin, and S. Tripathy, "Mechanism of enhanced light output efficiency in InGaN-based microlight emitting diodes," J. Appl. Phys. **93**(10), 5978–5982 (2003).
10. F. Olivier, A. Daami, C. Licitra, and F. Templier, "Shockley-Read-Hall and Auger non-radiative recombination in GaN based LEDs: A size effect study," Appl. Phys. Lett. **111**(2), 022104 (2017).
11. X. H. Wang, W. Y. Fu, P. T. Lai, and H. W. Choi, "Evaluation of InGaN/GaN light-emitting diodes of circular geometry," Opt. Express **17**(25), 22311–22319 (2009).
12. L. Zhang, F. Ou, W. C. Chong, Y. Chen, and Q. Li, "Wafer-scale monolithic hybrid integration of Si-based IC and III–V epi-layers—A mass manufacturable approach for active matrix micro-LED micro-displays," J. Soc. Inf. Disp. **26**(3), 137–145 (2018).
13. G. Harbers, S. J. Bierhuizen, and M. R. Krames, "Performance of high power light emitting diodes in display illumination applications," J. Disp. Technol. **3**(2), 98–109 (2007).
14. C. A. Bower, M. A. Meitl, B. Raymond, E. Radauscher, R. Cok, S. Bonafede, D. Gomez, T. Moore, C. Prevatte, B. Fisher, R. Rotzoll, G. A. Melnik, A. Fecioru, and A. J. Trindade, "Emissive displays with transfer-printed assemblies of 8 μm × 15 μm inorganic light-emitting diodes," Photon. Res. **5**(2), A23–A29 (2017).
15. G. Tan, J. H. Lee, S. C. Lin, R. Zhu, S. H. Choi, and S. T. Wu, "Analysis and optimization on the angular color shift of RGB OLED displays," Opt. Express **25**(26), 33629–33642 (2017).
16. R. H. Horng, H. Y. Chien, K. Y. Chen, W. Y. Tseng, Y. T. Tsai, and F. G. Tarn Tair, "Development and fabrication of AlGaInP-based flip-chip micro-LEDs," IEEE J. Electron Devi. **6**, 475–479 (2018).

17. Z. Liu, K. Wang, X. Luo, and S. Liu, "Precise optical modeling of blue light-emitting diodes by Monte Carlo ray-tracing," Opt. Express **18**(9), 9398–9412 (2010).
18. M. Moser, R. Winterhoff, C. Geng, I. Queisser, F. Scholz, and A. Dörnen, "Refractive index of $(Al_xGa_{1-x})_{0.5}In_{0.5}P$ grown by metalorganic vapor phase epitaxy," Appl. Phys. Lett. **64**(2), 235–237 (1994).
19. S. J. Lee, "Analysis of light-emitting diodes by Monte Carlo photon simulation," Appl. Opt. **40**(9), 1427–1437 (2001).
20. R. Hunt, *Measuring Colour*, 4th ed. (John Wiley & Sons, 2011).
21. M. D. Fairchild, *Color Appearance Models*, 3rd ed. (Wiley, 2013).
22. Y. D. Qi, H. Liang, D. Wang, Z. D. Lu, W. Tang, and K. M. Lau, "Comparison of blue and green InGaN/GaN multiple-quantum-well light-emitting diodes grown by metalorganic vapor phase epitaxy," Appl. Phys. Lett. **86**(10), 101903 (2005).
23. J. S. Lee, J. Lee, S. Kim, and H. Jeon, "GaN light-emitting diode with deep-angled mesa sidewalls for enhanced light emission in the surface-normal direction," IEEE Trans. Electron Dev. **55**(2), 523–526 (2008).
24. C. C. Kao, H. C. Kuo, H. W. Huang, J. T. Chu, Y. C. Peng, Y. L. Hsieh, C. Y. Luo, S. C. Wang, C. C. Yu, and C. F. Lin, "Light-output enhancement in a nitride-based light-emitting diode with 22° undercut sidewalls," IEEE Photonics Technol. Lett. **17**(1), 19–21 (2005).
25. K. Tomoda, N. Hirao, and G. Biwa, "Light emitting unit and display device", US patent 8,686,447 B2 (April 1, 2014).
26. C. S. McCamy, H. Marcus, and J. G. Davidson, "A color-rendition chart," J. Appl. Photogr. Eng. **2**(3), 95–99 (1976).
27. J. A. Dobrowolski, B. T. Sullivan, and R. C. Bajcar, "Optical interference, contrast-enhanced electroluminescent device," Appl. Opt. **31**(28), 5988–5996 (1992).
28. Y. Huang, G. Tan, F. Gou, M. C. Li, S. L. Lee, and S. T. Wu, "Prospects and challenges of mini-LED and micro-LED displays," J. Soc. Inf. Disp. **27**, 1–15 (2019), doi:10.1002/jsid.760.
29. A. Ohmae, Y. Kataoka, I. Nishinaka, T. Ohasha, G. Sakoda, and G. Biwa, "Light emitting apparatus, light emitting unit, display apparatus, electronic device and light emitting element," US patent 10,168,004 B2 (Jan. 1, 2019).
30. B. Pyo, C. W. Joo, H. S. Kim, B. H. Kwon, J. I. Lee, J. Lee, and M. C. Suh, "A nanoporous polymer film as a diffuser as well as a light extraction component for top emitting organic light emitting diodes with a strong microcavity structure," Nanoscale **8**(16), 8575–8582 (2016).
31. Z. Gong, S. Jin, Y. Chen, J. McKendry, D. Massoubre, I. M. Watson, E. Gu, and M. D. Dawson, "Size-dependent light output, spectral shift, and self-heating of 400 nm InGaN light-emitting diodes," J. Appl. Phys. **107**(1), 013103 (2010).
32. C. C. Lin, Y. H. Fang, M. J. Kao, P. K. Huang, F. P. Chang, L. C. Yang, and C. I. Wu, "Ultra-fine pitch thin-film micro LED display for indoor applications," SID Int. Symp. Digest Tech. Papers **49**(1), 782–785 (2018).
33. Y. Zhao, S. H. Oh, F. Wu, Y. Kawaguchi, S. Tanaka, K. Fujito, J. S. Speck, S. P. DenBaars, and S. Nakamura, "Green semipolar ($2\,0\,\overline{2}\,\overline{1}$) InGaN light-emitting diodes with small wavelength shift and narrow spectral linewidth," Appl. Phys. Express **6**(6), 062102 (2013).